Cancer Cell, Volume *41*

Supplemental information

TIM-3 blockade in diffuse intrinsic pontine glioma models promotes tumor regression and antitumor immune memory

Iker Ausejo-Mauleon, Sara Labiano, Daniel de la Nava, Virginia Laspidea, Marta Zalacain, Lucía Marrodán, Marc García-Moure, Marisol González-Huarriz, Irati Hervás-Corpión, Laasya Dhandapani, Silvestre Vicent, Maria Collantes, Iván Peñuelas, Oren J. Becher, Mariella G. Filbin, Li Jiang, Jenna Labelle, Carlos A.O. de Biagi-Junior, Javad Nazarian, Sandra Laternser, Timothy N. Phoenix, Jasper van der Lugt, Mariette Kranendonk, Raoull Hoogendijk, Sabine Mueller, Carlos De Andrea, Ana C. Anderson, Elizabeth Guruceaga, Carl Koschmann, Viveka Nand Yadav, Jaime Gállego Pérez-Larraya, Ana Patiño-García, Fernando Pastor, and Marta M. Alonso

Supplementary Data

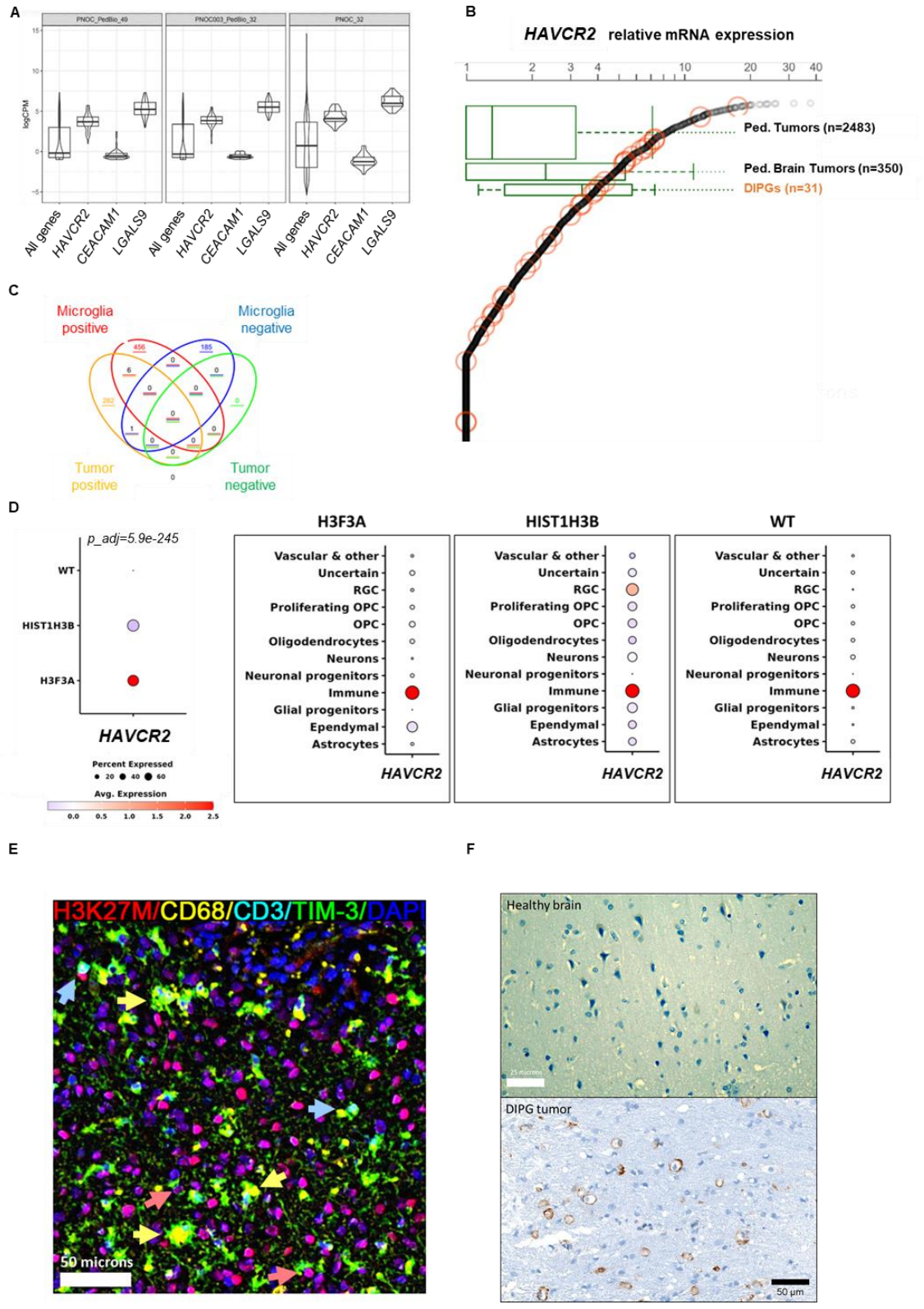

Figure S1. Characterization of HAVCR2 (TIM-3) expression in samples from DIPG patients, related to Figure 1. (A) Box plots showing mRNA expression of *HAVCR2*

and its ligands *LGALS9* and *CEACAM1* in DIPG patient samples. The lower and upper hinges correspond to the first and third quartiles. After stat (middle): median, 50% quantile, as well as the kernel density estimates as the width. **(B)** Box plots showing relative mRNA expression of TIM-3 (*HAVCR2)* in a cohort from St. Jude´s that includes all types of pediatric solid tumors (Ped Tumors (n=2483), pediatric brain tumors (Ped Brain Tumors (n=350), and DIPGs (n=31); top/bottom hinges: first and third quartiles, midline median, whiskers: max/min values) **(C)** Venn diagram showing the genes that significantly correlate with TIM-3 in microglia and in tumor cells, being only 6 common in both. Data obtained from single-cell RNA seq. **(D)** Dot plot showing TIM-3 expression in DIPG patient samples depending of H3 status. Data obtained from a previous patient's scRNA-seq dataset (n=66). **(E)** Representative image of a human DIPG tumor samples showing multiplex IF analyses of TIM-3, H3K27M (tumor cells), CD68 (macrophages and microglia) and CD3 (T cells). **(F)** Representative TIM-3 IHC analyses of a healthy brain (without TIM-3 expression) and a DIPG tumor sample from a patient.

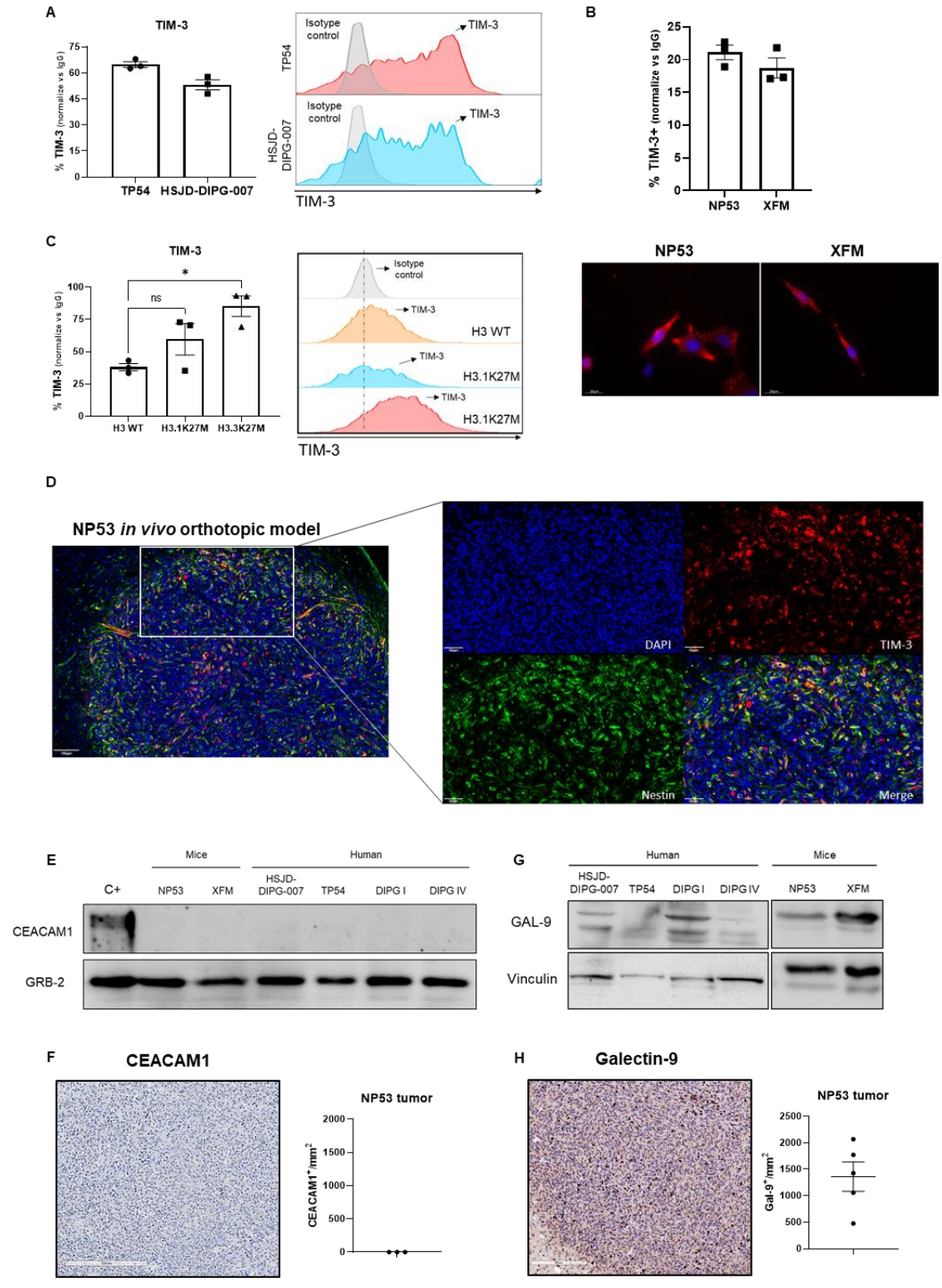

Figure S2. Evaluation of TIM-3 expression in murine and human cell lines, related to Figure 2. (A) *Left panel*, TIM-3 expression analyses by flow cytometry in TP54 and HSJD-DIPG-007. *Right panel*, representative flow cytometry histograms of TIM-3 MFI in TP54 and HSJD-DIPG-007. **(B)** *Up panel***,** Flow cytometry analysis of percentage of

TIM-3 expression in NP53 and XFM. *Down panel* Representative images of TIM-3 expression in NP53 and XFM murine cell lines by IF (scale bar, 20 μm). **(C)** Flow cytometry analysis of percentage of TIM-3 expression in H3WT, H3.1K27M and H3.3K27M cell lines **(D)** Mice were engrafted orthotopically with NP53 cells, sacrificed 10 days later and the brains were subjected to multiplexed immunofluorescence analysis to detect TIM-3 and Nestin markers. The nuclei were counterstained with DAPI. Representative images (scale bar, 50 μm) are shown. **(E)** Western blot analysis of CEACAM1 expression in DIPG human and murine cell lines, using GRB-2 as housekeeping. **(F)** *Left panel*, representative images of CEACAM1 expression levels in NP53 (scale bar, 200 μm). *Right panel*, quantification of CEACAM1+ cells per mm^2 of NP53 tumors (n=5). **(G)** Western blot analysis of galectin-9 expression in DIPG human and murine cell lines, using vinculin as housekeeping **(H)** *Left panel*, representative images of galectin-9 expression levels in NP53 (scale bar, 200 μm). *Right panel*, quantification of galectin-9+ cells per mm^2 of NP53 tumors (n=5). Bar graphs indicate the mean ± SEM.

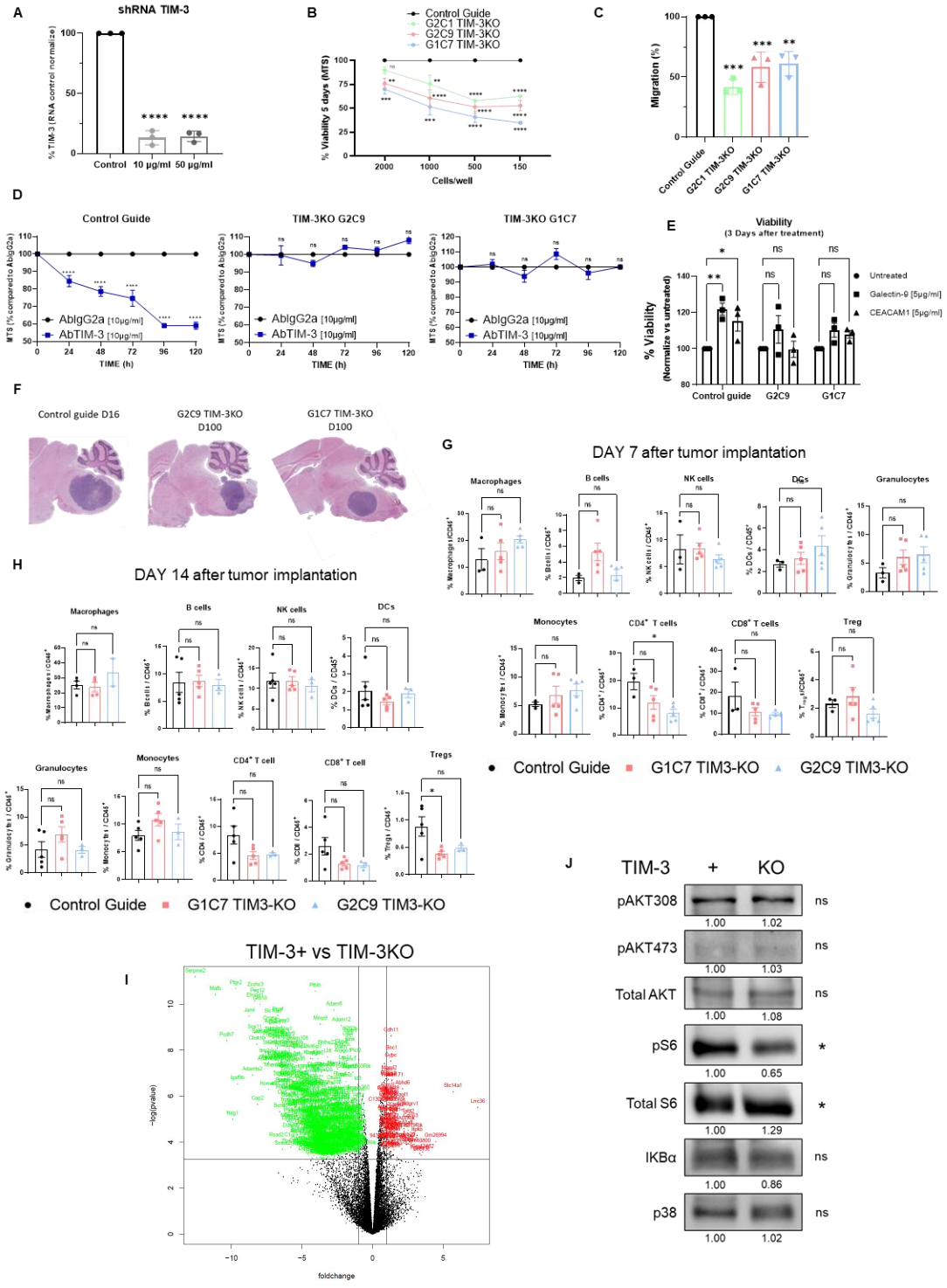

Figure S3. TIM-3 role in the tumor cell in vivo is not due to changes in the immune microenvironment but in its own metabolism, related to Figure 2. (A) Percentage of RNA TIM-3 expression in TP54 human DIPG cell line 72h after 10 µg/ml and 50 µg/ml doxycycline activation of the inducible TIM-3 shRNA normalize versus control. **(B)**

Viability assay (MTS) of control guide and TIM-3KO NP53 with different number of cells at day 5 after seed the cells. **(C)** Transwell migration assay comparing TIM-3+ and TIM-3 KO cell lines 16 hours after seed the cells. **(D).** Viability assay (MTS) of control guide and TIM-3KO NP53 treated with anti-TIM-3 (10µg/ml), or its corresponding IgG, every 24h up to 5 days. **(E)** Viability assay (MTS) of NP53 control guide, G2C9 and G1C7 TIM-3KO cells 3 days after treatment with galectin-9 and CEACAM1 (TIM-3 main ligands). **(F)** Representative hematoxylin/eosin staining images of mice bearing control guide or TIM-3KO NP53 tumors at the time of death (day 16) or at the end of the experiment (day 100). **(G)** Flow cytometry analysis of all immune populations in mice with NP53 control guide, G2C1 TIM-3KO or G2C9 TIM-3KO cells 7 days after tumor orthotopically implantation**. (H)** Flow cytometry analysis of all immune populations in mice with NP53 control guide, G2C1 TIM-3KO or G2C9 TIM-3KO cells 14 days after tumor orthotopically implantation**. (I)** Volcano plot of TIM-3+ and TIM-3KO NP53 cell line. Schematic representation of RNA-seq data. **(J).** Western blot analysis of AKT, pAKT308, pAKT473, S6, pS6, IkBα and p38 expression in TIM-3+ and TIM-3KO murine DIPG cell lines. Standardized quantification against its own vinculin (housekeeping) and a Student's t-test is performed for TIM-3+ versus TIM-3KO statistical analysis. Two-way ANOVA was performed on all graphs except for panels A and C (One-way ANOVA). Bar and line graphs indicate the mean ± SEM (ns, $P>0.05$; *$P<0.05$; **$P<0.01$; ***$P<0.001$; ****$P<0.0001$).

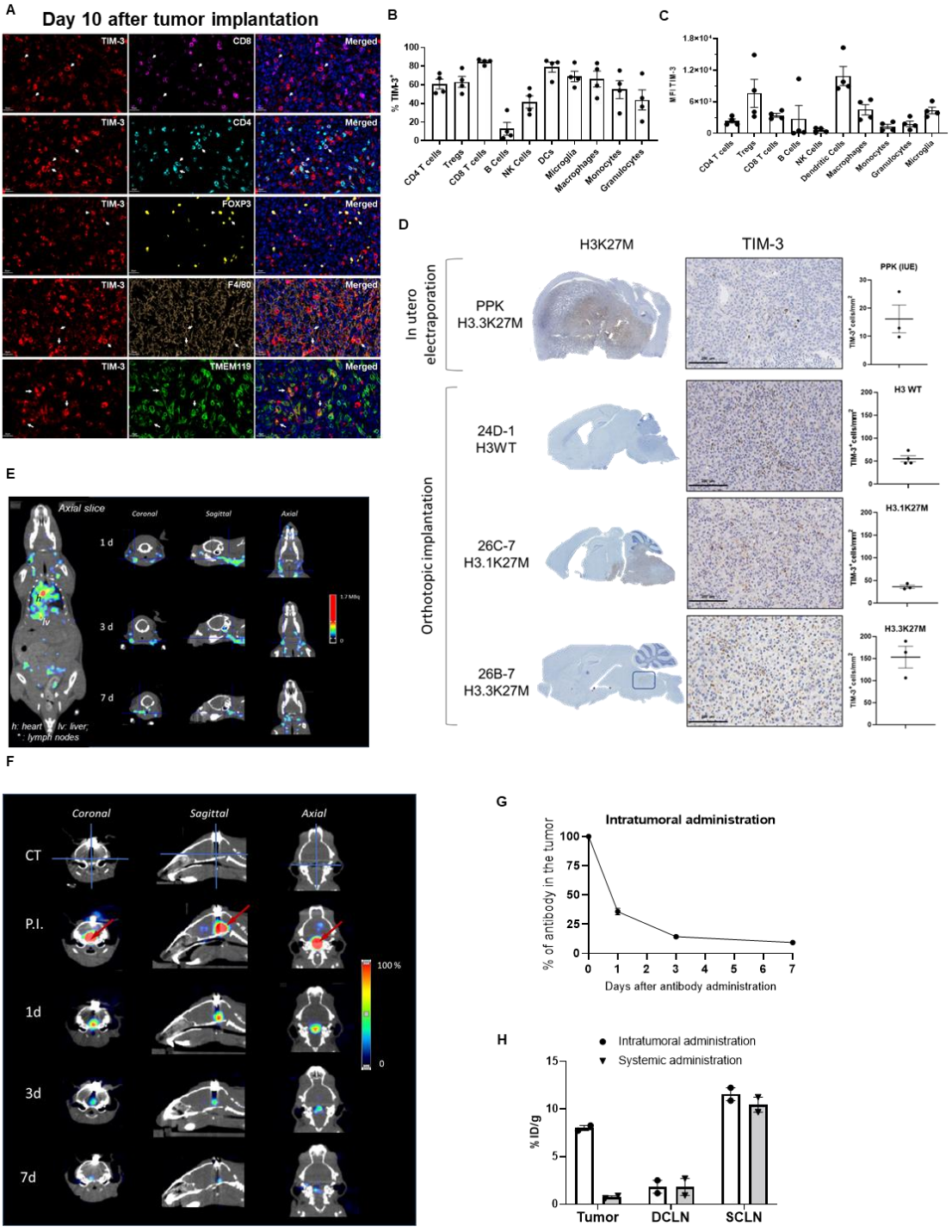

Figure S4. Characterization of TIM-3 expression and anti-TIM-3 biodistribution according to intratumoral or systemic administrations in murine immunocompetent models, related to Figure 3. (A) Mice were engrafted orthotopically with NP53 cells, sacrificed 10 days later and the brains were subjected to multiplexed immunofluorescence analysis to detect the following immune cells markers: TIM-3, TMEM119, F4/80, CD4

and FOXP3. The nuclei were counterstained with DAPI. Representative images (scale bar, 20 μm) are shown. **(B and C)** Mice were engrafted orthotopically with NP53 cells, sacrificed 10 days later, and the brains for flow cytometry analyses of TIM-3 expression in the indicated immune populations of the brain microenvironment. Data is shown as **(B)** percentage and **(C)** MFI of TIM-3 expression (n=4). Bar graphs indicate the mean ± SEM **(D)** Evaluation of TIM-3 expression in different DIPG models. (*Left panel*) Representative images of H3 mutational status in four different DIPG models (one in utero electroporation models and 3 orthotopic implantation models). (*Right panel*) TIM-3 expression representative images and quantification (TIM-3^+ cell per mm^2 of tumor). (scale bar, 200 μm) **(E)** Representative image of gallium67-labeled antibody biodistribution at day (d) 1, 3 and 7 after systemic administration. **(F)** Representative image of gallium67-labeled antibody biodistribution at day 1, 3 and 7 after intratumorally administration. **(G)** Quantification of the percentage of labelled antibody in the tumor 7 days after intratumoral administration (mean ± SEM). **(H)** Ex vivo quantification of weight-corrected dose percentage in tumor, deep cervical LN (DC LN) and superficial cervical LN (SC LN) comparing intratumoral and systemic administration (n=2). Bar graphs indicate the mean ± SEM

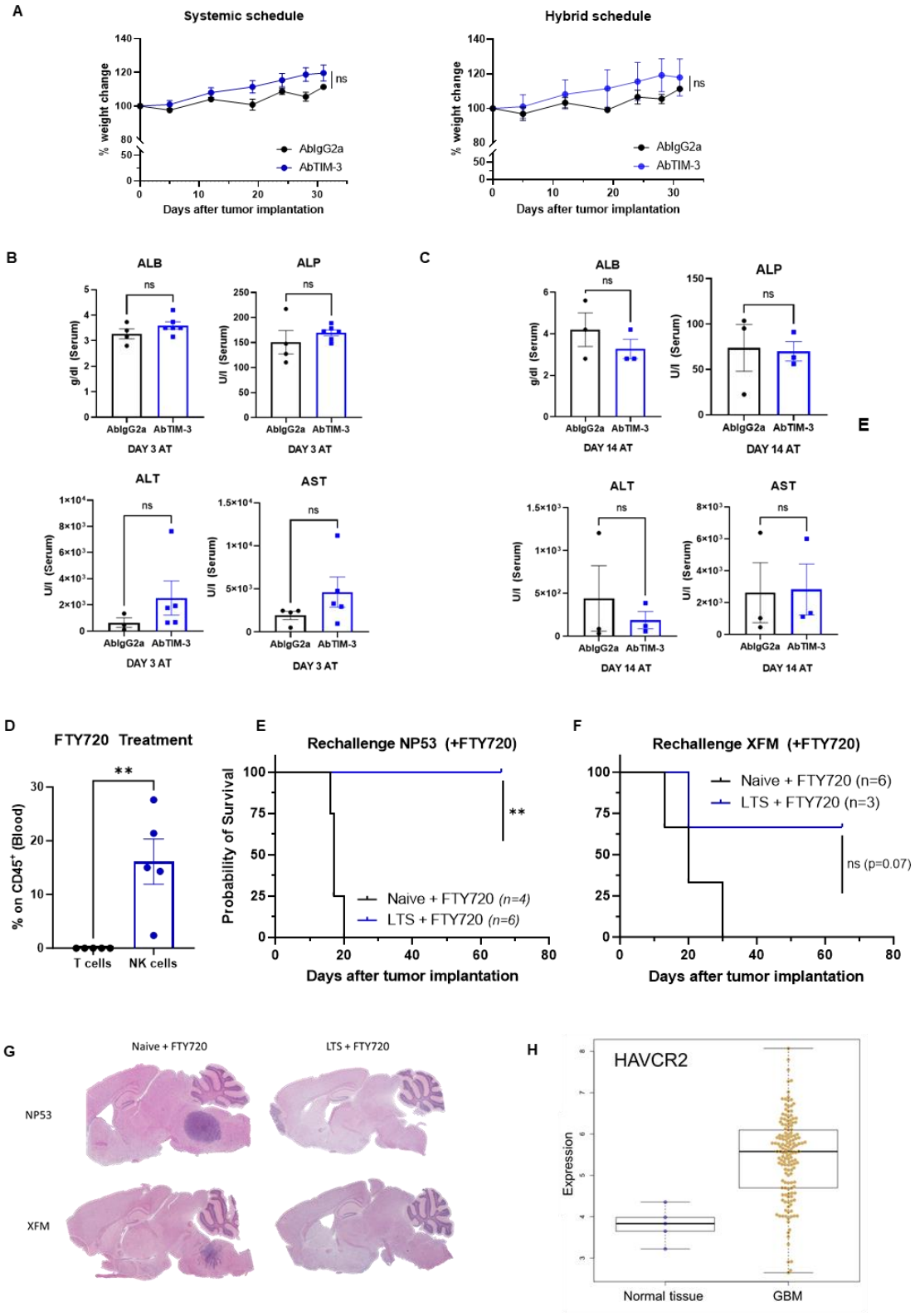

Figure S5. Assessment TIM-3 blockade toxicity in vivo and immunological memory characterization, related to Figure 3. (A) NP53 *fl/fl* mice bearing NP53 cells orthotopically were treated as indicated in the schedule with IgG2a or anti-TIM-3

antibody. Mice from the different groups (n=12, per group) were weighed every 3-4 days until day 30. *Left panel,* data are shown as the mean ± SEM of the systemic schedule within each group at each time point. *Right panel,* data are shown as the mean ± SEM of the hybrid schedule within each group at each time point. **(B and C)** Evaluation of biochemical parameters related to hepatic toxicity after hybrid treatment. Mice were treated with IgG2a or anti-TIM-3 and serum samples were collected **(B)** 3 and **(C)** 14 days later. Several parameters were measured, including alanine aminotransferase (ALT, U/L), aspartate aminotransferase (AST, U/L) and alkaline phosphatase (ALP, U/L) levels to monitor for hepatic injury and albumin (ALB, g/dL) levels to assess hepatic function. The student´s t test was performed. Bar graphs indicate the mean ± SEM (n=5). **(D)** Analyses of the percentage of T and NK cells in blood $CD45^+$ cells of mice treated with FTY720 **(E)** Kaplan-Meier survival plot of long-term survivors (LTS) TIM-3 treated mice that were subjected to a new rechallenge after administration of the FTY720 drug in the NP53 model (Naïve +FTY720 n=4 and LTS +FTY720=6). Log-rank p=0.001. **(F)** Kaplan-Meier survival plot of long-term survivors (LTS) TIM-3 treated mice that were subjected to a new rechallenge after administration of the FTY720 drug in the XFM model (Naïve +FTY720 n=6 and LTS +FTY720=6). Log-rank p=0.07. **(G)** Representative images of long-term survivors (LTS) or naïve mice bearing NP53 and XFM tumors at the time of death in the FTY720 survival experiment. **(H)** Box plots showing mRNA expression of HAVCR2 in GBM patients samples compared with normal tissue (TCGA cohort; top/bottom hinges: first and third quartiles, midline median, whiskers: max/min values). (ns, P>0.05; **P*<0.05; ***P*<0.01; ****P*<0.001; *****P*<0.0001).

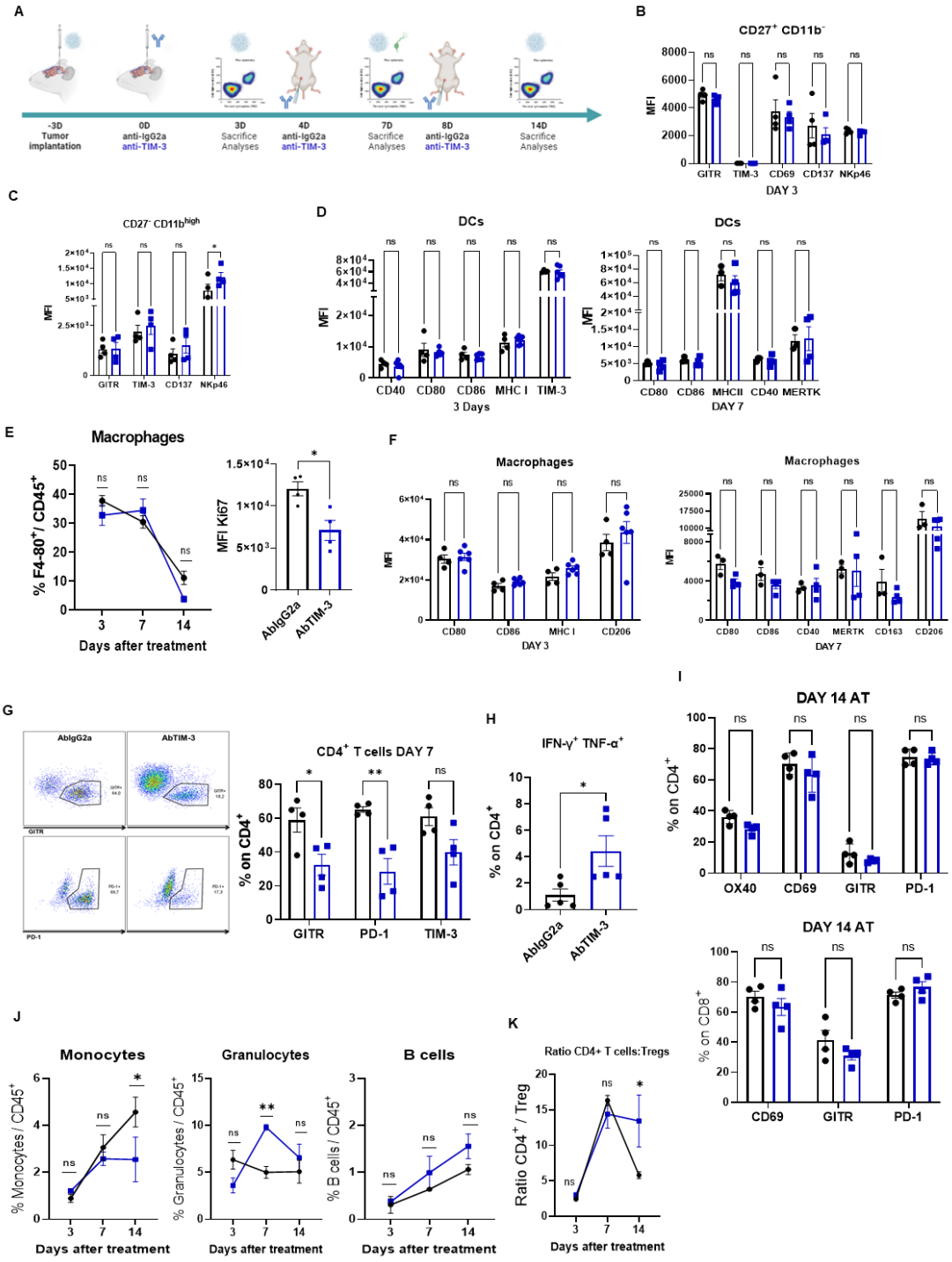

Figure S6. Characterization of the myeloid and lymphoid populations in the tumor microenvironment after TIM-3 blockade, related to Figure 4. (A) Schedule followed for the characterization of the different immune populations in the brains of mice bearing NP53 tumors on the indicated days after treatment with IgG2a or anti-TIM-3. **(B-C)** Analysis of **(B)** $CD27^{+}CD11b^{-}$ and **(C)** $CD27^{-}CD11b^{high}$ NK cells phenotype markers at

day 3 (n=4 per group). **(D)** MFI cytometry analyses of DCs maturation markers on days 3, and 7 after treatment (n=4 per group). **(E-F)** Flow cytometry analyses of macrophages (F4/80+) **(E)** percentage on $CD45^+$, $Ki67^+$ cells and **(F)** phenotype markers on the indicated days after treatment (n=4). **(G)** Flow cytometry analyses of different activation (GITR) and exhaustion (PD1, TIM-3) markers were performed in the $CD4^+$ subset at 7 days after i.t antibody administration (n=4). *Left panel*, representative image. *Right panel*, quantification of the expression expressed as the percentage on CD4+ T cells. **(H)** Flow cytometry analysis of TNF-α and IFN-γ expression after *ex vivo* stimulation of $CD4^+$ TILs treated with IgG2a or anti-TIM-3 (n=5). **(I)** Flow cytometry analyses of $CD4^+$ (*up panel*) and $CD8^+$ (*down panel*) T cells phenotype at day 14 after i.t. treatment. **(J)** Analyses of the percentage of monocytes, granulocytes, and B cells per $CD45^+$ on the indicated days (n=5; mean ± SEM). (**K)** Analyses of $CD4^+$ T cells: Treg ratio in the tumor microenvironment at days 3, 7, and 14 (mean ± SEM). Two-way ANOVA was performed on all graphs except F and H panel (Student´s t test). Bar graphs indicate the mean ± SEM (ns, P>0.05; *P<0.05; **P<0.01; ***P<0.001; ****P<0.0001).

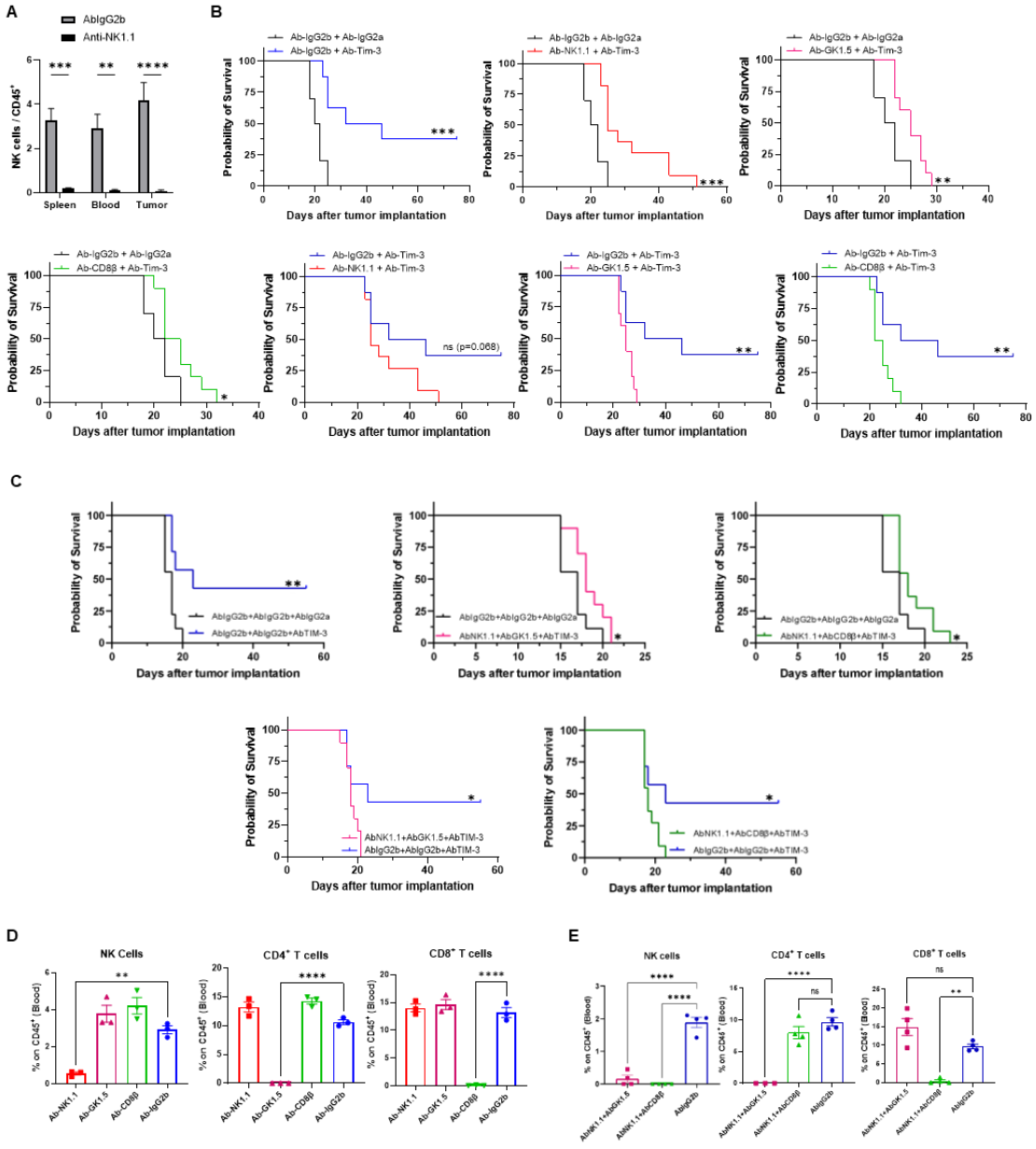

Figure S7. Assessment of the role of NK and T cells immune populations in the anti-TIM-3 efficacy, related to Figure 5. (A) FACS analysis of the percentage of NK cells in the spleen, blood and tumors of mice treated with the depletion NK antibody. **(B)** Kaplan-Meier survival plots of mice bearing NP53 cells (H3-mutated) treated with anti-TIM-3 antibody and NK cells, $CD4^+$ T cells and $CD8^+$ T cells depletion antibodies alone. **(C)** Kaplan-Meier survival plots of mice bearing NP53 cells treated with anti-TIM-3 antibody and a combination of NK cells+$CD4^+$ T cells and NK cells+$CD8^+$ T cells depletion. **(D-E)** FACS analysis of the percentage of NK, $CD4^+$ T cells and $CD8^+$ T cells

in the blood of mice treated with the depletion antibodies in both experiments. Two-way ANOVA was performed. Bar graphs indicate the mean ± SEM. One-way ANOVA was performed. Bar graphs indicate the mean ± SEM. (ns, $P>0.05$; *$P<0.05$; **$P<0.01$; ***$P<0.001$; ****$P<0.0001$).

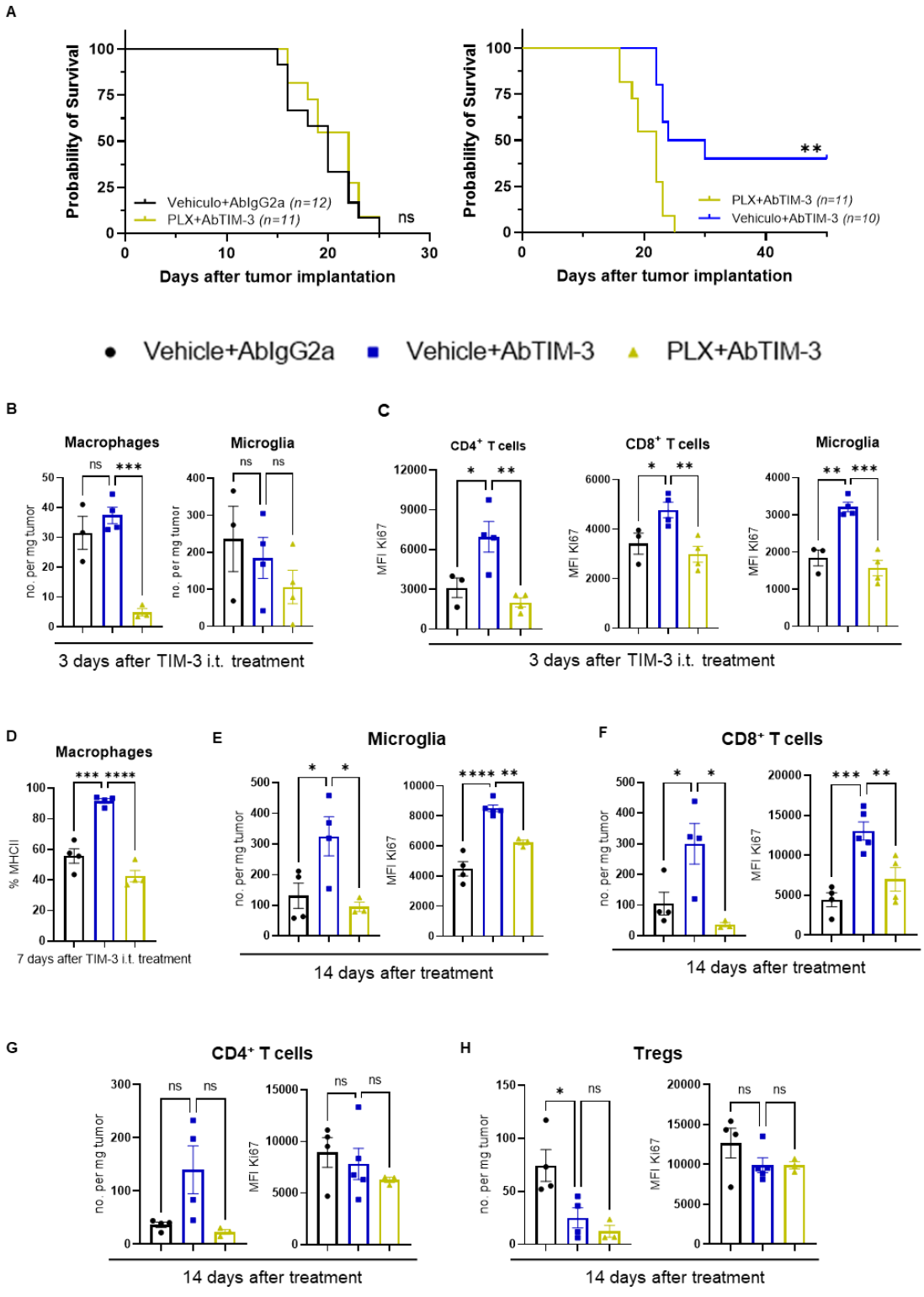

Figure S8. Assessment of the role of macrophages and microglia immune populations in the anti-TIM-3 efficacy, related to Figure 5. (A) Kaplan-Meier survival

plot mice bearing NP53 cells treated with anti-TIM-3 antibody or IgG2a and an anti-CSFR1 drug (PLX). One-way ANOVA was performed. **(B)** Flow cytometric analyses of macrophages and microglia number of cells per mg tumor on day 3 in the indicated groups **(C)** Flow cytometric analyses of Ki67 MFI on microglia, $CD4^+$ and $CD8^+$ T cells, 3 days after anti-TIM-3 i.t. treatment. **(D)** Flow cytometric analyses of MHCII expression in macrophages on day 7 after treatment. **(E)** Flow cytometric analyses of microglia number of cells per mg tumor (*left panel*) and Ki67 MFI (*right panel*) on day 14 in the three treatment groups. **(F)** Flow cytometry analyses of $CD8^+$ number of cells per mg tumor (*left panel*) and Ki67 MFI (*right panel*) comparing Vehicle+AbIgG2a, Vehicle+AbTIM-3 and PLX+AbTIM-3 groups on the indicated day. **(G)** Flow cytometric analyses of $CD4^+$ number of cells per mg tumor (left panel) and Ki67 MFI (right panel) on day 14 in the three treatment groups. **(H)** Flow cytometric analyses of Tregs number of cells per mg tumor (left panel) and Ki67 MFI (right panel) on day 14 in the three treatment groups. Bar graphs indicate the mean ± SEM. (ns, P>0.05; *P<0.05; **P<0.01; ***P<0.001; ****P<0.0001).

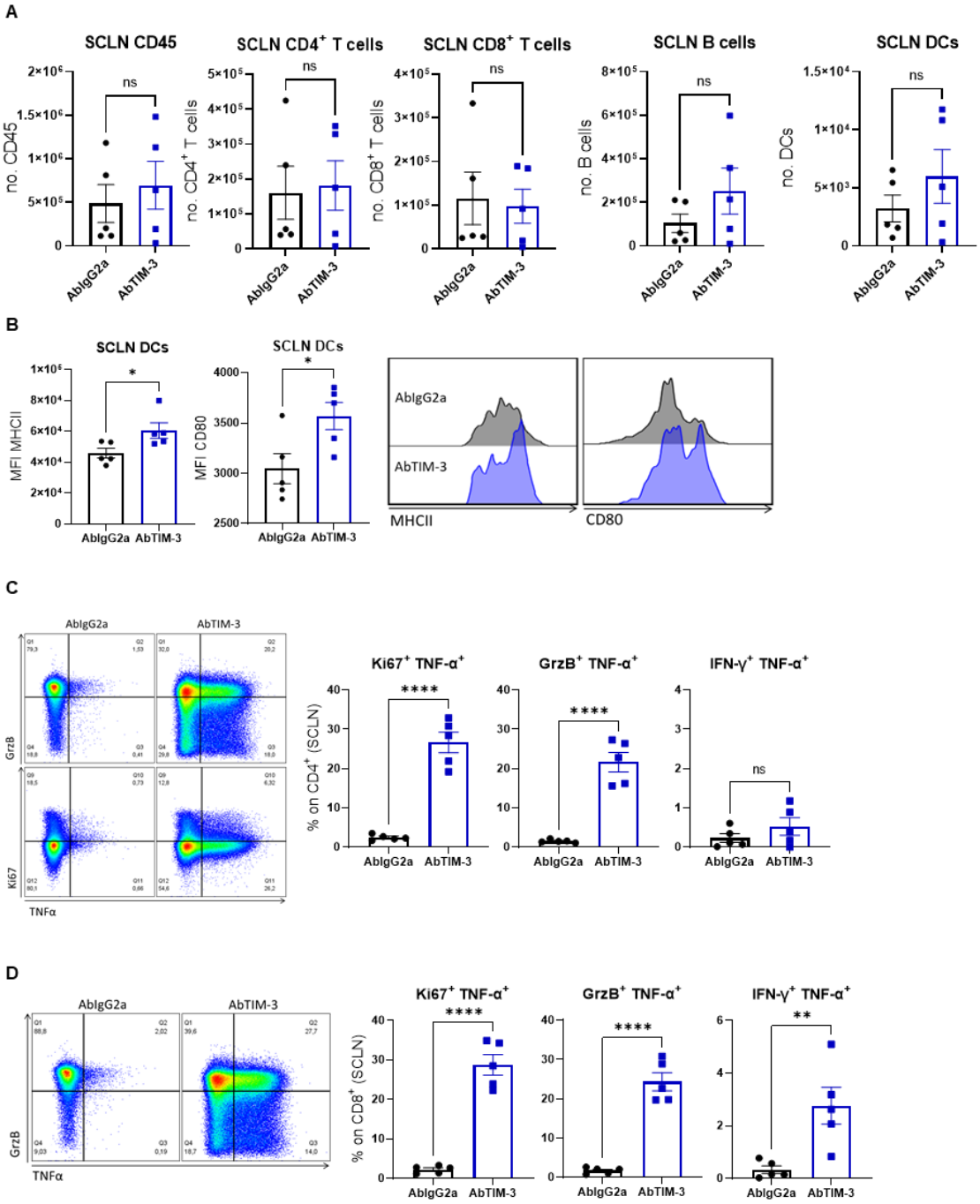

Figure S9. Assessment of the role of superficial cervical tumor-draining lymph nodes in TIM-3 blockade, related to Figure 6. Characterization of the composition of the superficial cervical tumor-draining lymph nodes of mice bearing NP53 tumors on the indicated days after treatment with IgG2a or anti-TIM-3. **(A)** Flow cytometry analyses of the number of $CD45^+$, $CD4^+$ T cells, $CD8^+$ T cells, B cells and DCs of superficial cervical LN (SC LN) seven days after i.t. treatment (n=5). **(B)** MFI analysis of MHCII

and CD80 expression on superficial cervical LN DCs at day 7. (**C and D)** Flow cytometry analysis of Ki67, TNF-α, GrzB, and IFN-γ expression after ex vivo stimulation of **(C)** $CD4^+$ and **(D)** $CD8^+$ T cells from superficial cervical LN treated with IgG2a or anti-TIM-3. The student´s t test was performed on all graphs. Bar graphs indicate the mean ± SEM (ns, P>0.05; *P<0.05; **P<0.01; ***P<0.001; ****P<0.0001).

A

H3 mutation and TIM-3 expression in the IHC analysis

Patient	AP_ID	Age (years)	Sex	Histone K27M - % of mutation	% TIM-3	
					Tumor positive	Immune positive
V02	2018B00213.svs	8	F	H3F3A – 36%	43,22	56,64
V04	2018B02705.svs	9	F	H3F3A – 27%	44,72	47,88
V05	2018B05423.svs	3	F	H3F3A – 33%	27,87	49,40
V06	2018B06717.svs	9	M	H3F3A – 42%	45,30	40,07
V07	2018B08699.svs	3	F	H3F3A – 12%	37,69	41,64
V07	2018B08736.svs	3	F	H3F3A – 12%	46,62	34,57
V10	2019B07991.svs	9	F	HIST1H3B – 18%	40,28	43,92
V11	2019B10121.svs	15	M	H3F3A – 35%	39,55	39,55
V12	2020B00727.svs	11	M	H3F3A – 31%	43,07	43,55
V08	DIPG-V8.svs	18	F	Not detected (WT)	43,88	53,70

B

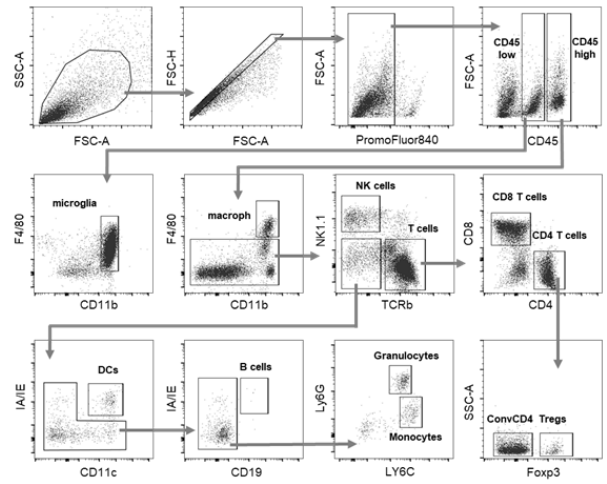

Fluorochrome	Target
PrCPC5.5	Ly6G
FITC	Ly6C
PE-Cy7	CD11c
AF700	CD45
APC	F4/80
BV421	CD19
BV510	CD8
BV605	NK1.1
BV650	IA/IE
BV785	TCRb
BUV395	CD11b
BUV496	CD4
PE-eFluor610	Foxp3
IR840	viability

C

H3 status of patients from the PNOC RNAseq analysis.

Patient ID	AGE	Sex	Histone K27M - % of mutation
PT_M23Q0DC3	4	F	H3-3A - 31%
PT_9GKVQ9QS	5	F	H3-3A - 44%
PT_KBFM551M	9	M	H3WT
PT_V1HNAC2Q	7	M	H3-3A - 42%
PT_NK8A49X5	13	M	H3-3A - 47%
PT_KZ56XHJT	7	F	H3-3A - 61%
PT_QA9WJ679	14	M	H3-3A - 43%
PT_0MXPTTM3	25	M	H3WT
PT_HGM20MW7	9	M	H3-3A - 22%
PT_M9XXJ4GR	10	M	H3-3A - 47%
PT_KTRJ8TFY	5	M	H3-3A - 39%
PT_1E3E6GMF	6	F	H3F3A - 36%
PT_VPEMAQBN	4	F	H3C2 - 40%
PT_7P6J57H3	5	M	H3-3A - 64%
PT_MNSEJCDM	5	M	H3C3 - 37%
PT_V1HNAC2Q	7	M	H3-3A - 42%
PT_WGVEF96B	7	F	H3-3A - 44%
PT_C5FKRB1P	12	M	H3WT
PT_CSKHQB16	3	F	H3C2 - 41%
PT_1AAYYGGY	12	M	H3F3A - 46%
PT_NWYSD53S	4	F	H3-3A - 36%
PT_8P368R5B	12	F	H3WT
PT_814K3T0D	7	M	H3F3A – NA%
PT_C9YDTZPA	5	M	H3-3A - 53%
PT_KAQMYFYB	6	M	H3-3A - 93%
PT_Y74CVASJ	4	F	H3-3A - 47%
PT_W5GP3F6B	6	M	H3-3A - 44%
PT_A06JR0E5	6	M	H3F3A - 40%
PT_EN2RN5Y1	8	F	H3-3A - 27%
PT_DMAF1J4A	6	M	H3-3A - 48%
PT_RYMG3M91	10	F	H3-3A - 45%
PT_RE6AXQM1	4	M	H3-3A - 49%
PT_G16VK7FR	5	F	H3C2 - 41%
PT_1YQH5NSH	6	M	H3-3A - 39%
PT_G9A050X1	11	M	H3WT
PT_R5T773FS	7	M	H3-3A - 42%
PT_FKCPVY7V	11	F	H3-3A - 45%
PT_6VD8J6FB	18	F	H3F3A (G34R)-62%
PT_TVJ5EGMR	10	M	H3WT
PT_5K5CZXYB	14	F	H3WT
PT_MV5WXTQV	6	M	H3WT
PT_V482NWB8	11	F	H3-3A - 28%
PT_WMWFCG6J	14	M	H3WT
PT_YRNATR8Q	9	F	H3WT
PT_ZTWCA9HX	20	F	H3WT
PT_0EBP2PBD	7	F	H3F3A - 53%
PT_4B34NTJB	8	F	H3WT
PT_8SF8D0M9	NA	M	H3-3A - 27%
PT_3QFBAXAN	NA	F	H3-3A - 45%
PT_C86SGM7B	NA	F	H3-3A (G34R) - 63%
PT_Z2KHR3GQ	NA	F	H3-3A - 60%
PT_9GKVQ9QS	5	F	H3F3A - 40%

D

Single-cell RNAseq analysis

H3 status	Samples	% of patients
H3F3A	49	74,24%
HIST1H3B	9	13,64%
H3WT	8	12,12%

Figure S10. Information about DIPG patients used in the different analyses, related to STAR methods. (A) Table with the patient´s age and histone 3 mutations status regarding the samples used in the IF staining for TIM-3 in figure 1I and Figure S1E and

S1F **(B)** Flow gating strategy used for all tumor microenvironment immune population characterization experiments. **(C)** Table with data on the age and H3 mutational status of the PNOC patients included in the analysis of TIM-3 expression and other immune markers**. (D)** Table with histone 3 mutation information of the patients used in the single-cell RNAseq analysis.